Advanced Materials

ADVANCED MATERIALS
www.advmat.de

RESEARCH ARTICLE OPEN ACCESS

Breaking the 2-nm Barrier in Hard Disk Drives Using Monolayer Amorphous Carbon Overcoats

Hongji Zhang[1,2] | Artem K. Grebenko[2] | Dmitrii Litvinov[1,3] | Wenwen Zheng[1] | Konstantin V. Iakoubovskii[2] | Sergey Y. Grebenchuk[3] | Anna Makarova[4] | Alexander Fedorov[4,5,6] | Andrei Starkov[3] | Carlo M. Orofeo[1] | Denis V. Vyalikh[7,8] | Mario Lanza[1,3] | Maciej Koperski[1,3] | Kostya S. Novoselov[1,3] | Chee-Tat Toh[1,2,9] | Barbaros Özyilmaz[1,2,3,9]

[1]Department of Materials Science and Engineering, National University of Singapore, Singapore, Singapore | [2]Department of Physics, National University of Singapore, Singapore, Singapore | [3]Institute for Functional Intelligent Materials, National University of Singapore, Singapore, Singapore | [4]Helmholtz-Zentrum Berlin für Materialien und Energie, Berlin, Germany | [5]Leibniz Institute for Solid State and Materials Research, Dresden, Germany | [6]Joint Laboratory "Functional Quantum Materials" at BESSY II, Berlin, Germany | [7]Donostia International Physics Center (DIPC) Donostia-San, Sebastián, Spain | [8]IKERBASQUE, Basque Foundation for Science, Bilbao, Spain | [9]Centre for Advanced 2D Material Singapore, National University of Singapore, Singapore, Singapore

Correspondence: Barbaros Özyilmaz (barbaros@nus.edu.sg)

Received: 28 September 2025 | **Revised:** 9 January 2026 | **Accepted:** 19 January 2026

Keywords: 2D material | amorphous carbon | carbon overcoat | hard disk device

ABSTRACT

The rapid growth of artificial intelligence (AI) has increased the demand for large-scale data storage, making hard disk drives (HDDs) indispensable in data centers due to their cost-effectiveness and stability. To support AI-driven data requirements, increasing the areal storage density is critical. However, this metric is increasingly constrained by the carbon overcoat (COC), the essential protective layer for magnetic media. Traditional diamond-like carbon (DLC) can no longer fulfill the stringent demands for ultrathin coatings and high thermal stability required by next-generation technologies like Heat-Assisted Magnetic Recording (HAMR) and bit-patterned media. Here, we introduce monolayer amorphous carbon (MAC) as a superior alternative. MAC is directly grown on the heterogeneous (Fe, Pt, SiO_2) HDD surface at low temperatures (~ 300°C), achieving an uniform 0.8 nm thickness across 2.5-inch disks. Despite its atomic thickness, MAC demonstrates high corrosion resistance and low roughness comparable to commercial 2.5 nm COCs. Its fully amorphous, sp^2-hybridized structure ensures excellent thermal stability under HAMR-like conditions (~450°C) and a low friction coefficient, enabling potential lubricant-free operation. Replacing traditional COCs with MAC facilitates the development of HDD media capable of achieving 10 Tb/in^2, addressing the urgent storage demands of the digital era.

1 | Introduction

Rapid advances in deep learning, generative models, and large-scale data analytics drive a massive demand for data storage infrastructure. Global data generation is expected to reach 175 zettabytes, and the latest forecast by the International Data Corporation (IDC) anticipates a rapid increase to 393.9 zettabytes by 2028 [1, 2]. As AI model complexity and dataset sizes grow exponentially [3, 4], magnetic hard disk drives (HDDs) are increasingly recognized as one of the few workable solutions

Hongji Zhang and Artem K. Grebenko contributed equally to this work.

for large-scale storage due to their cost-effectiveness and high stability. However, storing these vast amounts of data leads to a significant increase in physical footprint and power consumption [5]. Therefore, technologies like heat-assisted magnetic recording (HAMR) [6], which provide higher storage density, are essential to minimise device counts and energy use in storage centers.

Higher areal density imposes significant challenges on traditional HDD technology [7–9]. The IEEE roadmap identifies the carbon overcoat (COC) as a component requiring critical advances [7]. The COC protects the magnetic recording layer from corrosion, mechanical wear, and head crashes. Theoretical calculations suggest reducing the COC thickness to below 1 nm for both magnetic media and read-heads could increase the areal density towards 10 Tb/in^2 [10, 11]. Despite this potential, commercial COC thickness has only decreased from 3 to 2.5 nm over the past decade [10]. Conventional COCs use diamond-like carbon (DLC) with mainly sp^3 hybridized content. The out-of-plane nature of sp^3 bonds makes it a significant challenge to achieve a continuous film below 1 nm [12, 13]. The presence of the COC now sets a fundamental limit on areal density.

First, the head-media spacing (HMS) must be reduced to accommodate smaller magnetic bits and weaker magnetic signals. For current HDDs with areal density ~1.4 Tb/in^2, the total HMS for hard disk media is ~6.5–8.9 nm.This distance comprises of the head COC (1.5–2 nm), the flying height (2–3.2 nm), the lubricant (1–1.2 nm) and the media COC (2–2.5 nm) [10]. Second, the superparamagnetic limit affects smaller magnetic bits [14]. To overcome the size limit, magnetic materials with higher coercivity, such as FePt, are required for stable information storage [6]. Writing to these materials requires techniques like HAMR to locally heat magnetic bits above their Curie point (Figure 1a) [6, 14–16]. These high temperatures, especially when paired with rapid changes, pose significant challenges for commercial COCs [15, 17–19]. The sp^3 carbon in DLC graphitizes under these conditions, leading to cracks during operation. Increasing sp^3 content reduces graphitization but does not eliminate it [20]. Graphene has emerged as a potential alternative due to its high thermal stability [21]. While promising results were reported with transferred graphene [22], direct growth at low temperature has not yet been established.

Third, traditional COCs require a lubricant layer to lower the friction coefficient between the magnetic media and head. Thermal depletion of the lubricant and its volume within the HMS reduce storage density and shorten the HDD lifetime. Recent theoretical findings suggest that sp^2-rich amorphous carbon can reduce friction coefficients down to superlubricant conditions [32].

We propose monolayer amorphous carbon (MAC) to overcome these limitations. We synthesize MAC directly on the heterogenous hard disk media surfaces at low temperatures. This process yields an atomically thin, uniform film with high mechanical strength and corrosion resistance. The continuous sp^2 network provides excellent thermal stability and a low friction coefficient. Replacing traditional COCs with MAC enables the next generation of high-density HAMR technology.

2 | Result and Discussion

2.1 | Basic Characterization of MAC Grown on HDD

The growth substrate used in this work is a platter of commercially available 2.5-inch HDD (Figure S1). Such hard disk platters are coated with a layer of lubricant and a COC, as illustrated in Figure 1a. We follow Reuben et al. to remove in situ the COC and lubricant to obtain pristine bare metal disks by Ar^+ plasma cleaning prior to the growth of MAC [23]. Removal of the lubricant and COC layer is confirmed by cross-sectional electron energy loss spectroscopy (EELS) mapping (Figure S2). We further show, using atomic force microscopy (AFM) analysis, that the structural damage of both the etching and growth processes is negligible. The roughness values of the commercial disk, as purchased (0.17 nm) and after the growth of MAC (0.18 nm), are comparable (Figure 1b; Figure S2). Moreover, magnetic force microscopy (MFM) mapping of the HDD also shows that the typical domain structures is preserved after the growth of the MAC layer (Figure 1c; Figure S2).

The thickness of the as-grown MAC film was directly measured by cross-sectional transmission electron microscopy (TEM, Figure 1f). The MAC layer is uniform and continuous, as shown in Figure 1d, and zoomed-in images confirm a monolayer thickness of 0.8 nm (Figure 1f), compared to the 2.5 nm thickness of traditional COC (Figure 1g). X-ray photoelectron spectroscopy (XPS) measurements of the as-grown MAC film confirm its sp^2 structure (Figure S4), and the Raman spectrum shows an I(D)/I(G) ratio of 0.8 (Figure S4), suggesting that the MAC prepared in this work is structurally similar to previously reported MAC grown on Cu [24, 25]. The thickness uniformity over the entire hard disk surface is examined by ellipsometry mapping and shows a variance of ~0.2 nm across the entire 2.5-inch disk. Growth conditions followed the previously reported approach of laser-plasma-assisted CVD with carbon precursor (see Materials and Methods and Figure S5).

2.2 | Anti-Corrosion Performance of MAC

The data storage layer contains alloys of transition metals such as Co, Fe, and Cr, which are chemically active and unstable against corrosion [26]. Therefore, one of the main functions of COC is to prevent such degradation. The efficiency of corrosion suppression of as-grown MAC was characterized using a standard 3-cell electrochemical test and compared to the bare disk and commercial COC-protected hard disk. The measurements were done in 0.1 M NaCl electrolyte with saturated Ag/AgCl as reference electrode and Pt as counter electrode, following the previous procedure by Dwivedi et al. [22]. The test area for each scan was about 0.25 cm^2 randomly chosen across the entire hard disk (see Figure S6).

When metal contacts a corrosive solution, metal ions are released into the liquid while electrons are generated at the surface (Figure 2a). The reverse process occurs at the cathode, where metal ions in solution gain electrons and are reduced. During electrochemical corrosion tests, both anodic and cathodic sweeps were performed by ramping the potential and recording the

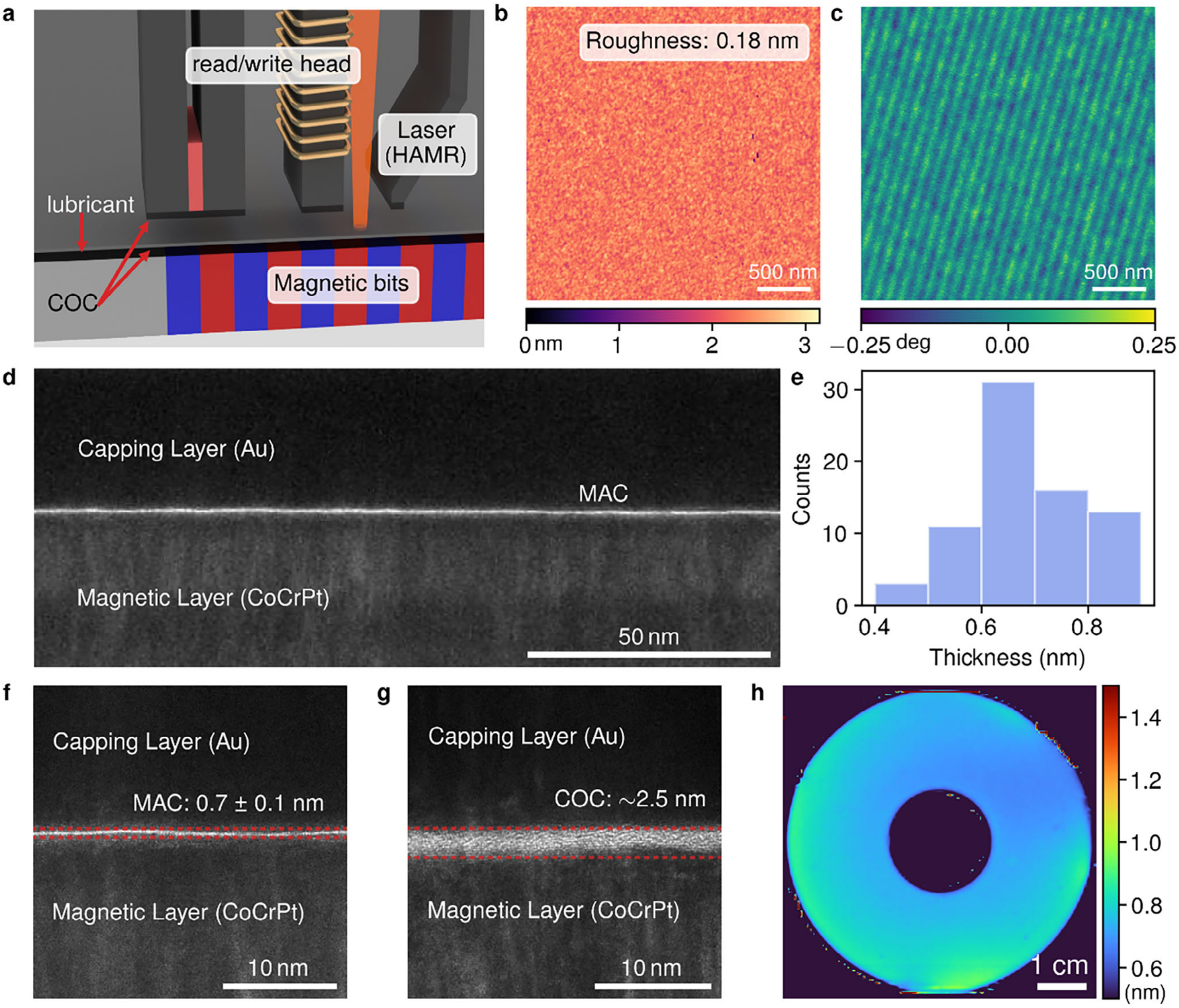

FIGURE 1 | Characteristics of HDDs with directly grown monolayer amorphous carbon overcoating. (a) Schematic illustration of the HAMR device zoomed at the head (including laser)/media interface. Magnetic bits are indicated by blue and red stripes with a protective COC layer (black) and lubricant (gray) on top. (b) AFM surface topography image used for roughness analysis of as-grown MAC on hard disk (RMS ~ 0.18 nm). (c) Phase contrast MFM image of a hard disk after MAC growth, clearly showing ordered magnetic bit lines. (d) Large view cross-sectional TEM image of as-grown MAC on HDD capped with an Au layer. (e) Histogram of the thickness distribution obtained from multiple TEM images (see Figure S3). (f) Zoom-in cross-sectional TEM image of as-grown MAC showing a thickness of 0.8 nm. (g) Zoom-in cross-sectional TEM image of a commercially purchased hard disk with COC showing a thickness of 2.5 nm. (h) Ellipsometry mapping of MAC thickness across the entire 2.5-inch disk surface showing a thickness variation smaller than 0.2 nm.

current with a potentiostat. To extract figures of merit, we used Tafel plots (Figure 2b). The corrosion current density J_{corr} was determined by linearly extrapolating the anodic and cathodic branches of the Tafel plot and identifying their intersection point, as shown in Figure S6. For each sample tested, at least three sweeps were performed to ensure the stability and reliability of the data. As a result, we obtained a corrosion current density of ~22 nA/cm^2 for the bare disk and ~4.3 nA/cm^2 for the COC-coated hard disk, which matched previous reports [22].

Since the corrosion reaction entails the transfer of electrons and ions between the metal and solution, the corrosion rate depends directly on the corrosion current. The corrosion protection efficiency (CPE) is then defined as how efficiently the coating can protect the hard disk against corrosion [22]:

$$CPE\,(\%) = \frac{J_{corr}^{Bare} - J_{corr}}{J_{corr}^{Bare}} \times 100\%$$

where J_{corr}^{Bare} is the corrosion current density for the bare hard disk and J_{corr} refers to a protected hard disk. The calculated results show that despite the monolayer thickness of the MAC film, the corrosion current is ~3.8 ± 0.1 nA/cm^2, which gives a CPE of 82.7%, a performance comparable to that of a 2.5 nm thick commercial COC, previously reported DLC coatings, and outperforms even 4-layer thick transferred graphene films [22]. (Figure 2c).

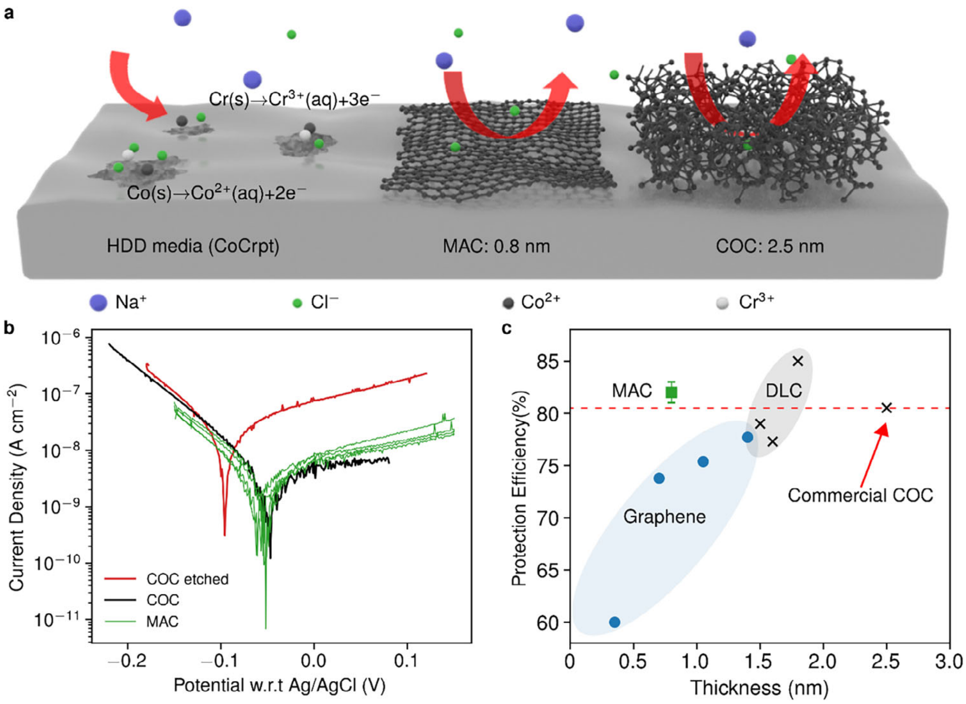

FIGURE 2 | Electrochemical corrosion test of bare and coated hard disk media. (a) Schematic of some corrosion reactions possible in NaCl electrolyte and the protection function of COC. (b) Tafel plot for etched COC disk (red), COC-coated disk (black), and disk with MAC (green). (c) CPE of MAC compared to commercial COC, DLC, and transferred CVD graphene as a function of thickness [22, 23, 27, 28].

In addition, we performed complementary measurements at different pH values as well as under prolonged electrochemical treatment. The corresponding results are summarized in Figure S6.

2.3 | Thermal Stability Test Under HAMR Like Condition

In addition to its anti-corrosion properties, thermal stability is also essential for HAMR technology. During HAMR operation, magnetic bits are heated to around 750 K in less than 1 nanosecond using an infrared laser [15], reaching the Curie temperature of FePt, so the bit's state can be changed. It is important that the carbon coating (COC) remains stable at high temperatures and can withstand the rapid heating and cooling cycles [26, 27]. To test the thermal stability of MAC, we checked its structure after irradiating the sample with an 800 nm femtosecond pulsed laser similar to the one used by John et al. for HAMR magnetic switching (see Figure S7) [28]. We also studied the impact of the laser power on the graphitization of the COC, with power ranging from 0 to 12 mW, which corresponded to a max intensity of 18 mJ/cm^2 per pulse. An intensity of 15 mJ/cm^2 is enough to flip the magnetization without damage [28]. Given the 80 MHz repition rate and 85 fs pulse duration, 15 s of irradiation yields a ~ 100 µs cumulative exposure. This total irradiation time simulates the cumulative laser exposure expected over a five-year HDD lifetime [29].

After the exposure, we measured the Raman spectrum using a 532 nm green laser with a power of ~ 0.1 mW. Our setup allowed measurements of the Raman spectrum exactly at the same spot, thanks to the alignment of the laser beams. This power value is tested and known to be low enough to avoid any additonal damage to the film during measurements (Figure S7b). The measured Raman spectra for commercial COC and as-grown MAC are shown in Figure 3a,b. For each value of the infrared laser power, we have used a new position to avoid accumulated damage to the film.

For the commercial COC, two clear changes were detected in the Raman spectrum. First, the commercial COC exhibits a significant increase in the I(D)/I(G) ratio (Figure 3c), which is associated with graphitization. In addition, although less pronounced, a shift of the G band toward higher wave numbers was also observed(Figure 3c). Both phenomena indicate clustering and modification of the sp^2 phase in the structure [30, 31]. In contrast, MAC does not show any obvious structural change as indicated by the Raman spectrum, suggesting that its thermal stability is suitable for HAMR applications. Overall, conventional hydrogenated DLC overcoats are stable up to ~300–350°C, advanced ta-C or doped DLC formulations can tolerate ~450–500°C [30, 31].Graphene exhibits even higher intrinsic thermal stability [21].Notably, MAC demonstrates thermal robustness approaching this upper envelope.

2.4 | Investigation of Friction at the Interface

During the operation of the hard disk, occasional contact between the read head and the magnetic media is unavoidable. To minimize mechanical damage to the media, a lubricant is usually used to reduce friction. Therefore, COC should either provide a high affinity to lubricants to prevent their depletion during

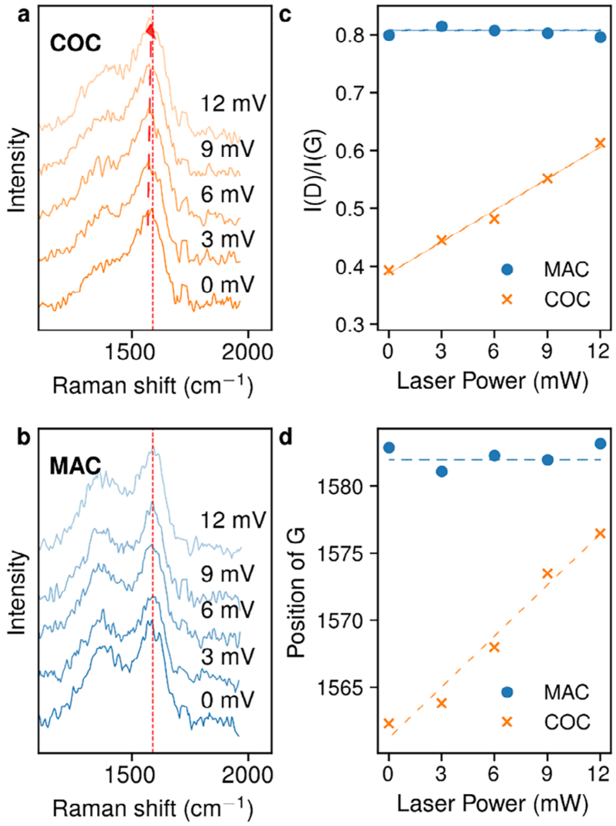

FIGURE 3 | Thermal stability test of commercial COC and MAC subjected to 800 nm laser radiation with Raman spectroscopy analysis. (a) Raman spectrum of COC after laser irradiation from 0 mW (not treated) to 12 mW. (b) Raman spectrum of MAC after laser irradiation from 0 mW (not treated) to 12 mW. (c) I(D)/I(G) ratio for MAC and COC after laser treatment. (d) Position of the G band for MAC and COC after laser treatment.

operation or have a low coefficient of friction (COF). It is worth noting that for a disordered sp^2-hybridized amorphous carbon, superlubricity has been predicted [32].

For HDD operation, typically a COF of 0.2–0.3 is required. Since commercial COCs have a friction coefficient of up to 0.5, a lubricant is necessary [33]. In this work, the friction between various surfaces was characterized by lateral force microscopy (LFM) using a SiO_2 ball tip as illustrated in the inset of Figure 4a. Even though the read head is commonly made of Al_2O_3, studies done by Hiratsuka et al. have shown that when measured in an air environment, the COF of Al_2O_3 against various metals is similar to that of SiO_2 (with a discrepancy of less than 0.1) [34]. In our experiments, we used two different tips: one was an as-purchased SiO_2 ball, and the other was a SiO_2 ball coated with MAC.

During the friction test, the spring constant of the cantilever was calibrated using the thermal tune method. This is a standard technique available in most modern AFMs for converting the raw voltage signal into the applied normal force F_N. For each friction test, an area of 10 μm^2 was scanned for both trace and retrace. (Figure 4a,b) To avoid contributions from topographical features naturally occurring during scanning, the friction signal was obtained from half of the difference between the lateral force microscopy (LFM) signals recorded during trace and retrace (Figure 4c) [35]. To obtain the friction force F_f from the raw voltage signal V_{lat}, several calibration steps were performed to calculate the sensitivity S_Φ (voltage signal to torsional deflection, V/rad) and torsional spring constant k_Φ (Nm/rad). The friction force can then be calculated by $F_f = S_\Phi\, k_\Phi\, V_{lat}/H$, where H is the height of the AFM tip. We followed an approach first proposed by Sader et al., which allows estimation of S_Φ and k_Φ within 10–20% accuracy [36, 37]. (Figure S8)

To extract the coefficient of friction (COF), we obtained surface-averaged values of the lateral force as a function of the applied normal load. All measurements followed the classical linear Amontons-Coulomb law $F_f = \mu F_N$. The scanning rate was fixed at 10 μm/s to minimize contributions from the stick-n-slip effect. As shown in Figure 4a,b, lateral force maps were free of any steps and kinks. For the bare disk, we obtained a COF of~0.6, whereas a COC with lubricant covered HDD exhibited a lower COF of ~0.28, consistent with previously reported values [21]. The friction coefficient between MAC and SiO_2 was ~ 0.41, which limits its application with non-covered heads. However, the COF of MAC-coated media (without lubricant) against MAC-coated SiO_2 was as low as 0.27. Remarkably, this value is comparable to COC with lubricant. This value remains stable over 15,000 repeated cycles along the same scan line in the LFM experiment, indicating good tribological stability at the nanoscale. Even though macroscopic friction and wear tests under HDD-relevant conditions are still required, the present results provide a strong motivation for advancing toward full-disk fabrication and testing. While transferred graphene can enable even lower friction coefficients [21], directly grown MAC exhibits advantageous mechanical characteristics, including stronger adhesion to the growth substrate [38] and high mechanical fracture toughness [39], which are critical for the robustness of ultra-thin overcoats.

3 | Conclusions

In summary, we demonstrate that monolayer amorphous carbon (MAC) functions as an ultra-thin, robust, and thermally stable protective overcoat for hard disk drives, breaking the long-standing ~2 nm thickness barrier for carbon-based coatings. Direct growth of MAC onto commercial HDD media provides corrosion resistance comparable to conventional 2.5 nm diamond-like carbon (DLC) films, while reducing the overcoat thickness to 0.8 nm. MAC further preserves its structural and chemical integrity under HAMR-relevant thermal stress.

Beyond the disk overcoat, our results indicate that replacing the conventional carbon overcoat on the read head with MAC could enable sufficiently low friction to allow lubricant-free HDD operation. This offers a pathway to further reducing the head–media spacing and mitigating lubricant depletion in HAMR systems. Together, these findings establish MAC as a promising material for pushing the limits of areal density in next-generation HDD technologies.

From a manufacturing perspective, the process meets key requirements for industrial translation, including scalability, throughput, and compatibility with double-sided disk coating. The growth approach is scalable to at least 4-inch disk

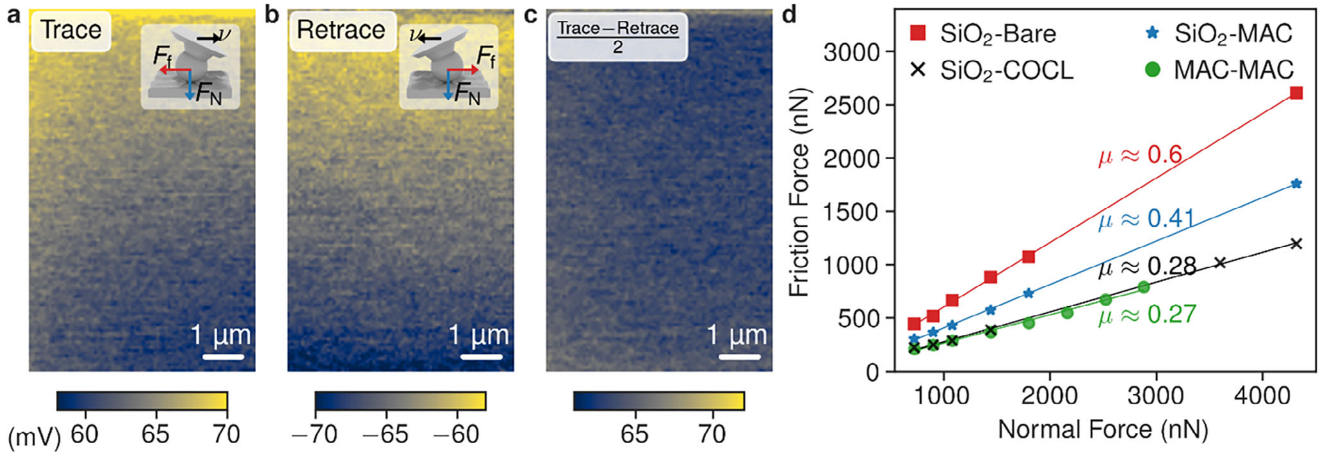

FIGURE 4 | Coefficient of Friction analysis by LFM. (a) Trace scan map of lateral force measured by LFM. (b) Retrace the scan map of the lateral force measured by LFM. (c) Calculated plot of (Trace-Retrace)/2, in whicn the non-uniformity caused by sample slope is removed. (d) Plot of lateral force vs. normal force applied. The slope of the trend line reflects the coefficient of friction for the corresponding interfaces.

substrates as it relies on uniform plasma/photochemical activation and surface-limited growth. While current growth times are on the order of minutes, they are already within one order of magnitude of industrial targets and are expected to be reduced through further optimization, without exceeding the HAMR thermal budget, as the growth temperature of 300°C is fully compatible with established manufacturing constraints [40, 41].

Looking forward, integration of MAC overcoats offers a clear pathway toward continued scaling of magnetic data storage. More broadly, the combination of sub-nanometer thickness, thermal stability, and effective barrier performance positions MAC as a compelling material for other technologies requiring ultra-thin protective layers, including nanoscale sensors, advanced optoelectronics, and photonic devices.

4 | Materials and Methods

4.1 | Synthesis

The hard disk platters were taken from commercial 5 TB Seagate hard disk drives, each containing five platters. During the growth, one platter was loaded into the CVD chamber, mounted on a Cu foil. The CVD chamber was pumped to the base pressure of 7×10^{-5} mBar. Ar gas was then introduced into the chamber with a flow rate of 70 sccm. The pressure was controlled by a butterfly valve and stabilized at 3×10^{-2} mBar. A DC plasma was then generated at 50 V and 3W for 2 min for the etching of the surface lubricant and COC. After the etching process, the plasma setup was changed to a remote setting in situ. The CVD chamber was again pumped to the base pressure. During the growth process, 20 sccm of CH_4 gas was passed through the CVD chamber while maintaining a pressure of 3×10^{-2} mBar. The temperature of the stage was raised up to 250°C for uniform growth over the entire surface. To generate required growth species, 248 nm laser with an energy of 220 mJ per pulse and a frequency of 50 Hz was irradiated on the Cu foil underneath the platter while not directly irradiating the surface of the platter. The final temperature of the substrate was measured to be 300°C. A DC plasma of 80 V and 5 W was used to generate the plasma environment. The total growth time was 10 min. Control experiments without plasma or without Cu foil resulted in incomplete film formation and poor electrochemical performance (Figure S5).

4.2 | TEM Lamellae Preparation and Analysis

TEM lamellae were prepared using a standard lift-out procedure with a Helios G4 UX FIB system (Thermo Fisher Scientific), equipped with a Ga^+ ion beam source. High-resolution TEM (HRTEM), high-angle annular dark-field scanning TEM (HAADF-STEM) imaging, energy-dispersive X-ray spectroscopy (EDS) mapping, and electron energy loss spectroscopy (EELS) were performed using FEI Titan Cs Probe and FEI Titan ST transmission electron microscopes.

4.3 | Ellipsometry

MAC-COC thickness was mapped by spectroscopic ellipsometry using an Accurion EP4 spectrometer equipped with a computer-controlled x-y stage. The angle of the incident light was 60°, and the spatial resolution was 0.6 mm.

4.4 | Electrochemical Tests

Electrochemical tests were performed with a standard three-cell setup and a Keithley 6430 as a potentiostat to control the potential and measure the current. The electrolyte was a 0.1 M NaCl solution. The reference electrode was a saturated Ag/AgCl, and the counter electrode was Pt. The working electrode-hard disk pieces were fully covered by epoxy with only the test window exposed in the electrolyte for the measurement (Figure S6). The voltage was swept linearly with 1 mV per step at a number of power line cycles (NPLC) of 10.

4.5 | Raman Spectroscopy

Raman measurements were performed with a home-built confocal setup in a backscattering geometry. A 532 nm continuous-wave laser has been used for excitation. The laser beam was focused into a spot with a diameter of ca. 0.5 μm using a 100X/0.55 optical objective (Olympus M Plan Apo SL). The collected spectra were dispersed by a 0.75 m spectrometer (SpectraPro HRS-750, Princeton Instruments) coupled with a nitrogen-cooled visible CCD camera (PyLoN 100BRX, Princeton Instruments).

4.6 | Thermal Stability Measurements

For thermal stability experiments, a 785 nm pulsed laser has been used (Toptica FemtoFiber smart with a typical pulse width of 85 fs, laser spot of 0.9 μm, and repetition rate of 80 MHz). The exposure time was controlled by using a beam shutter (SH05R, ThorLabs). Power has been changed by rotation of a variable neutral density filter (NDC-100C, ThorLabs).

4.7 | X-ray Photoelectron Spectroscopy

Room temperature XPS (C 1*s* (Figure 3g)) was performed at the FlexPES beamline of the MAX IV synchrotron radiation facility. The measurements were performed for the annealed (≈500°C) samples of MAC on SiO_2/Si. All the spectra were pre- and post-edge normalized.

4.8 | Atomic Force Microscopy

Topography measurements were performed using Park NX-20 AFM operating in non-contact mode with Multi75AlG cantilevers by Budget Sensors.

Magnetic force microscopy (MFM) imaging of the magnetic bits in a hard disk after MAC growth was carried out in ambient conditions using Bruker Dimension Icon AFM in tapping-based dual pass mode. During the first pass, the topography of the sample was captured. Then the tip was lifted by 20 nm and tracked the z-profile captured during the first pass with the tip oscillating at resonant frequency. Magnetic interactions between the tip and substrate were recorded via the phase channel. We used MESP-V2 (Bruker, spring constant k∼3 N/m) tips covered with CoCr magnetic alloy. Before the measurements, the tip was magnetized using a permanent magnet.

Lateral Force Microscopy measurements were done using Park NX-20 AFM at ambient conditions. We used S-Qube CP-NCH-BSG-C-5 cantilevers with 10–130 N/m spring constant and 204–497 kHz resonant frequency. A 20 ± 2 μm SiO_2 ball was mounted on top of the cantilever beam. AFM was operated in a standard contact mode with lateral deflection detection enabled.

Author Contributions

H.Z. established a growth technique and performed an electrochemical test. H.Z. and A.S. fabricated samples. H.Z. and A.K.G. did LFM experiments, and D.L. and M.K. performed experiments to test the thermal stability of MAC and COC. W.Z. and M.L. performed cross-section TEM analysis of the films. K.V.I. did ellipsometry thickness mapping over HDD. S.Y.G. and M.K. performed MFM measurements. A.M., A.F. D.V.V. did XPS measurements of MAC on HDD. K.S.N. and M.K. supervised MFM and thermal stability experiments. C.M.O., C.T.T., and B. Ö. coordinated the project. B. Ö. Initiated and supervised the project. H.Z., A.K.G. and B. Ö. wrote the manuscript. All authors discussed the results and commented on the manuscript.

Acknowledgements

The authors are grateful to Nimura Kazuo and Lawrance Ng Wah from Fuji Electric for fruitful discussions at the early stages of the project. The authors are thankful to Dr. Lucas M. Sassi for helping in coordinating cross-sectional TEM samples experiments. B.Ö. acknowledges support by the National Research Foundation, Prime Minister's Office, Singapore, under its Competitive Research Programme (CRP award number NRF-CRP22-2019-008 and NRF-F-CRP-2024-0010), and Medium-Sized Centre Programme (CA2DM), by EDB Singapore, under its Space Technology Development Programme (S22-19013-STDP), and Research Centre of Excellence award to the Institute for Functional Intelligent Materials (I-FIM, Project No. EDUNC-33-18-279-V12). M. K. acknowledges support from the Ministry of Education, Singapore, under its Academic Research Fund Tier 2 (MOE-T2EP50122-0012) and Air Force Office of Scientific Research and the Office of Naval Research Global under award number FA8655-21-1-7026. M.B. acknowledges support by the Ministry of Education of Singapore, via Academic Research Fund Tier 2 (MOE-T2EP50122-0016). The authors acknowledge MAX IV Laboratory for experimental time on FlexPES beamline under Proposal No. 20231842. Research conducted at MAX IV, a Swedish national user facility, is supported by the Swedish Research Council under Contract No. 2018-07152, the Swedish Governmental Agency for Innovation Systems under Contract No. 2018-04969, and Formas under Contract No. 2019-0249. The authors thank the Helmholtz-Zentrum Berlin für Materialien und Energie for the allocation of synchrotron radiation beamtime at GELEM Dipole. The authors are grateful to Alexei Preobrajenski and Alexander Generalov, staff members at the FlexPES, for their strong interest and support of this research.

Conflicts of Interest

The authors declare no conflicts of interest.

Data Availability Statement

The data that support the findings of this study are available from the corresponding author upon reasonable request.

References

1. C. M and S. H J, "Secure Data Deduplication for Efficient Cloud Storage Using Blockchain Technologies," in 2024 7th International Conference on Circuit Power and Computing Technologies (ICCPCT), (IEEE, 2024).

2. R. Xie, L. Feng, Q. Tang, et al., "Delay-Prioritized and Reliable Task Scheduling With Long-Term Load Balancing in Computing Power Networks," *IEEE Transactions on Services Computing* 17 (2024): 3359–3372.

3. Z. Ghahramani, "Probabilistic Machine Learning And Artificial Intelligence," *Nature* 521 (2015): 452–459.

4. H. Wang, T. Fu, Y. Du, et al., "Scientific Discovery In The Age Of Artificial Intelligence," *Nature* 620 (2023): 47–60.

5. R. Nishant, M. Kennedy, and J. Corbett, "Artificial Intelligence For Sustainability: Challenges, Opportunities, And A Research Agenda," *International Journal of Information Management* 53 (2020): 102104.

6. W. A. Challener, C. Peng, A. V. Itagi, et al., "Heat-Assisted Magnetic Recording By A Near-Field Transducer With Efficient Optical Energy Transfer," *Nature Photonics* 3 (2009): 220–224.

7. T. Coughlin and R. Hoyt, "IEEE Roadmap Outlines Development of Mass Digital Storage Technology," *Computer* 57 (2024): 111–116.

8. G. Albuquerque, S. Hernandez, M. T. Kief, D. Mauri, and L. Wang, "HDD Reader Technology Roadmap to an Areal Density of 4 Tbpsi and Beyond," *IEEE Transactions on Magnetics* 58 (2022): 3100410.

9. E. Roddick, M. Kief, and A. Takeo, "2022 IEEE 33rd Magnetic Recording Conference (TMRC 2022)," (IEEE, 2022), pp. 1–2.

10. B. Marchon, T. Pitchford, Y.-T. Hsia, and S. Gangopadhyay, "The Head-Disk Interface Roadmap to an Areal Density of 4 Tbit/in^2," *Advances in Tribology* 2013 (2013): 521086.

11. R. J. Yeo, *Ultrathin Carbon-Based Overcoats for Extremely High Density Magnetic Recording*, (Springer, 2017).

12. A. C. Ferrari, "Diamond-Like Carbon For Magnetic Storage Disks," *Surface & Coatings Technology* 180–181 (2004): 190–206.

13. A. A. Balandin, M. Shamsa, W. L. Liu, C. Casiraghi, and A. C. Ferrari, "Thermal Conductivity Of Ultrathin Tetrahedral Amorphous Carbon Films," *Applied Physics Letters* 93 (2008): 043115.

14. L. Pan and D. B. Bogy, "Heat-Assisted Magnetic Recording," *Nature Photonics* 3 (2009): 189–190.

15. M. H. Kryder, E. C. Gage, T. W. McDaniel, et al., "Heat Assisted Magnetic Recording," *Proceedings of the IEEE* 96 (2008): 1810–1835.

16. N. Wang, K. Komvopoulos, F. Rose, and B. Marchon, "Structural Stability Of Hydrogenated Amorphous Carbon Overcoats Used In Heat-Assisted Magnetic Recording Investigated By Rapid Thermal Annealing," *Journal of Applied Physics* 113 (2013): 083517.

17. N. Wang and K. Komvopoulos, "Thermal Stability of Ultrathin Amorphous Carbon Films for Energy-Assisted Magnetic Recording," *IEEE Transactions on Magnetics* 47 (2011): 2277–2282.

18. M. T. Kief and R. H. Victora, "Materials For Heat-Assisted Magnetic Recording," *MRS Bulletin* 43 (2018): 87–92.

19. M. Rouhani, F. Chau-Nan Hong, and Y.-R. Jeng, "In-Situ Thermal Stability Analysis Of Amorphous Carbon Films With Different sp^3 Content," *Carbon* 130 (2018): 401–409.

20. K. Kim, W. Regan, B. Geng, et al., "High-Temperature Stability Of Suspended Single-Layer Graphene," *physica status solidi (RRL)–Rapid Research Letters* 4 (2010): 302–304.

21. N. Dwivedi, A. K. Ott, K. Sasikumar, et al., "Graphene Overcoats For Ultra-High Storage Density Magnetic Media," *Nature Communications* 12 (2021): 2854.

22. R. J. Yeo, E. Rismani, N. Dwivedi, et al., "Bi-Level Surface Modification Of Hard Disk Media By Carbon Using Filtered Cathodic Vacuum Arc: Reduced Overcoat Thickness Without Reduced Corrosion Performance," *Diamond and Related Materials* 44 (2014): 100–108.

23. C.-T. Toh, H. Zhang, J. Lin, et al., "Synthesis And Properties Of Free-Standing Monolayer Amorphous Carbon," *Nature* 577 (2020): 199–203.

24. H. Tian, Y. Ma, Z. Li, et al., "Disorder-Tuned Conductivity In Amorphous Monolayer Carbon," *Nature* 615 (2023): 56–61.

25. T. Liew, R. Ji, C. H. Seek, and T. C. Chong, "Corrosion Of Magnetic Recording Heads And Media," *Tribology International* 36 (2003): 447–454.

26. S. Xu, S. Sinha, E. Rismaniyazdi, C. Wolf, P. Dorsey, and B. Knigge, "Effect of Carbon Overcoat on Heat-Assisted Magnetic Recording Performance," *IEEE Transactions on Magnetics* 51 (2015): 3301805.

27. Y. S. Ma, Y. J. Man, M. Shakerzadeh, et al., "Laser-Heating-Induced Damage to Ultrathin Carbon Overcoat in Heat-Assisted Magnetic Recording," *Tribology Letters* 53 (2014): 303–310.

28. R. John, M. Berritta, D. Hinzke, et al., "Magnetisation Switching of FePt Nanoparticle Recording Medium By Femtosecond Laser Pulses," *Scientific Reports* 7 (2017): 4114.

29. R. Ji, Y. Ma, M. Shakerzadeh, H. L. Seet, and J. F. Hu, "Laser Irradiation Effect On Carbon Overcoat for HAMR Application," *Surface and Interface Analysis* 46 (2014): 204–208.

30. A. C. Ferrari and J. Robertson, "Interpretation Of Raman Spectra Of Disordered And Amorphous Carbon," *Physical Review B* 61 (2000): 14095.

31. A. C. Ferrari, J. Robertson, A. C. Ferrari, and J. Robertson, "Raman Spectroscopy Of Amorphous, Nanostructured, Diamond–Like Carbon, And Nanodiamond," *Philosophical Transactions of the Royal Society of London Series A: Mathematical, Physical and Engineering Sciences* 362 (2004): 2477–2512.

32. X. Li, N. Du, C. Feng, et al., "Theoretical Superlubricity And Its Friction Stability Of Amorphous Carbon Film Induced By Simple Surface Graphitization," *Applied Surface Science* 615 (2023): 156318.

33. N. Dwivedi, R. J. Yeo, P. S. Goohpattader, N. Satyanarayana, S. Tripathy, and C. S. Bhatia, "Enhanced Characteristics of Pulsed DC Sputtered Ultrathin (<2nm) Amorphous Carbon Overcoats On Hard Disk Magnetic Media," *Diamond and Related Materials* 51 (2015): 14–23.

34. K. Hiratsuka, A. Enomoto, and T. Sasada, "Friction and Wear of Al_2O_3, ZrO_2 and SiO_2 Rubbed Against Pure Metals," *Wear* 153 (1992): 361–373.

35. D. Martínez-Martínez, L. Kolodziejczyk, J. C. Sánchez-López, and A. Fernández, "Tribological Carbon-Based Coatings: An AFM and LFM Study," *Surface Science* 603 (2009): 973–979.

36. M. Munz, "Force Calibration In Lateral Force Microscopy: A Review Of The Experimental Methods," *Journal of Physics D: Applied Physics* 43 (2010): 063001.

37. X. Q. Koh, C. Thenarianto, V. Jokinen, and D. Daniel, "Quantifying Droplet–Solid Friction Using An Atomic Force Microscope," *Droplet* 3 (2024): 107.

38. H. Zhang, A. K. Grebenko, K. V. Iakoubovskii, et al., "Superior Adhesion of Monolayer Amorphous Carbon to Copper," *Advanced Materials* 37 (2025): 2419112.

39. B. Shin, B. Ni, C.-T. Toh, et al., "Intrinsic Toughening In Monolayer Amorphous Carbon Nanocomposites," *Matter* 8 (2025): 102000.

40. D. Tripathy, A. Ajan, T. SEKI, and G. A. Bertero, *Soft Underlayer for Heat Assisted Magnetic Recording Media* (2017): US9824711B1.

41. D. Weller, G. Parker, O. Mosendz, et al., "Review Article: FePt Heat Assisted Magnetic Recording Media," *Journal of Vacuum Science & Technology* 34 (2016): 060801.

Supporting Information

Additional supporting information can be found online in the Supporting Information section.

Supporting File: adma72281-sup-0001-SuppMat.docx.